THE JOURNAL OF PHYSICAL CHEMISTRY C

Article

Cite This: J. Phys. Chem. C 2018, 122, 24279−24286

pubs.acs.org/JPCC

Modeling the Impact of Metallic Plasmonic Resonators on the Solar Conversion Efficiencies of Semiconductor Photoelectrodes: When Does Introducing Buried Plasmonic Nanostructures Make Sense?

Paul A. Hernley and Suljo Linic*

Department of Chemical Engineering, University of Michigan, Ann Arbor, Michigan 48109, United States

Supporting Information

ABSTRACT: It is well established that plasmonic nanoparticles embedded in a semiconductor can, under certain conditions, increase the rate of charge carrier collection in electrocatalysts bound to the semiconductor surface by changing the depth at which photons are absorbed in the semiconductor. One mechanism that leads to this effect is the injection of photon energy into the semiconductor by near-field and scattering effects induced by plasmonic metal nanoparticles. It is also well-known that these metallic plasmonic materials are also photon absorbers that can dissipate the incident electromagnetic energy into heat, which can make them into relatively efficient parasitic absorbers. Therefore, it is not clear under what circumstances plasmonic nanostructures should enhance the quantum efficiencies of semiconductors. We have developed a physically transparent model to demonstrate when introducing buried plasmonic metal nanoparticles into semiconductors is beneficial to improving the photon conversion efficiency. The model captures the influence of the thickness, optical, and charge carrier transport properties of the semiconductor as well as the depth of the buried plasmonic metal nanoparticles. We demonstrate the utility of the model by probing the impact of buried metal plasmonic nanoparticles on the efficiency of three vastly different semiconductors: TiO_2, $BiVO_4$, and Si. Using this model, we recommend strategies for improving the efficiency of available semiconducting materials by introducing buried plasmonic antennas.

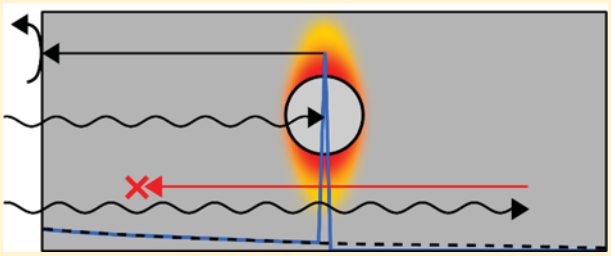

INTRODUCTION

The development of efficient ways to store solar energy in the form of chemical bonds is crucial for a sustainable future. A promising family of materials for this application is semiconductor light absorbers coupled with metal electrocatalysts at the surface of the semiconductor.[1−12] The generation of charge carriers through photon absorption in the semiconductor and the transport of these carriers to the reaction sites on the electrocatalysts are processes that must be efficient to achieve acceptable external quantum efficiencies (EQE).

In general, different semiconductors possess very diverse optical and charge transport properties that have a significant impact on the EQE. The reflectance of the semiconductor dictates the fraction of incoming light that enters the semiconductor, while the photon absorption depth dictates the fraction of photons absorbed by the semiconductor at a given depth. Once a photon is absorbed in the bulk of the semiconductor, the resulting charge carriers (electrons and holes) must be separated and transported to the reactive centers at the surface of semiconductor. Each semiconductor has a unique charge carrier diffusion length that corresponds to the distance a charge carrier can travel in the bulk before recombining. If a photon is absorbed at a depth away from the semiconductor surface that is greater than the charge carrier diffusion length, the charge carriers are likely to recombine before arriving at the reaction site. If the photon absorption depth is large relative to the electrode thickness, the EQE is limited by inefficient absorption. Both of these scenarios could be improved if photon absorption is enabled closer to the reaction centers (i.e., electrocatalysts at the semiconductor surface).

Metal nanoparticles can interact strongly with light of certain wavelengths as a result of localized surface plasmon resonance (LSPR). This excitation of LSPR results in strong electric fields near the surface of the particle. These electric fields can lead to the scattering of light by the particle to the far field or the absorption of light in the nanoparticle. The resonant wavelengths depend on the composition, size, and shape of the nanoparticles, as well as their local environment. Au and Ag nanoparticles can achieve these optical responses across the visible light spectrum.[13−20] There have been a number of examples demonstrating that these plasmonic, noble metal nanoparticles can be coupled with some semiconductors to enhance the EQE, particularly at the LSPR wavelengths.[21−26] It has been demonstrated that these enhancements are the result of a transfer of energy from the excited metal nanoparticles to the semiconductor, which leads to high rates of charge carrier generation in the semiconductor close to the

Received: July 26, 2018
Revised: October 3, 2018
Published: October 8, 2018

DOI: 10.1021/acs.jpcc.8b07214
J. Phys. Chem. C 2018, 122, 24279−24286

plasmonic nanoparticle.[21,22,27−29] These plasmon-induced enhancements of the EQE have, so far, been experimentally demonstrated mainly for semiconductors that have very short minority charge carrier diffusion lengths (such as Fe_2O_3 and doped TiO_2) and that, in general, exhibit relatively low EQEs.

While there are many reports of the positive impact of the plasmonic metal nanoparticles on the measured EQE, there are no clear, physically transparent guidelines about when these EQE enhancements should be expected and what their magnitude should be. We note that metallic nanoparticles are characterized by various pathways that lead to the parasitic loss of the light energy (i.e., heating of the nanoparticles). In light of these complexities, it is important to determine when and how plasmonic metal nanoparticles should be used in particular systems to improve the EQE of different families of semiconductors.[10,22,30,31] In this contribution, we present a simple, physically transparent photon conversion (PC) model that sheds light on the impact of plasmonic nanoparticles on the EQE of different families of planar semiconductor photoelectrodes. In our analysis we have focused on three different semiconductors (TiO_2, $BiVO_4$, and Si), which represent three different families of light absorbers in terms of the charge carrier diffusion and photon absorption lengths. The photon conversion (PC) model captures the optical (absorption, emission, and reflection) and bulk recombination properties of the semiconductor and evaluates the effect of placing idealized plasmonic metal nanoparticles at a specific depth in the planar semiconductor electrode.

THEORETICAL METHODS

The PC model, described in detail in the Supporting Information, is built upon compounding the probabilities of several processes that occur in series. For an incoming photon to be useful, it must enter the semiconductor, be absorbed at a specific depth, and generate electrons and holes that reach the active centers before recombining. For a pure semiconductor, these probabilities are respectively related to the wavelength-dependent reflectance of the semiconductor, photon absorption depth (inverse of the absorption coefficient), and effective charge carrier diffusion length. We describe the impact of plasmonic nanostructures embedded in a semiconductor by modeling them as "light concentrators", where these structures interact strongly with light. We assume that these materials can either efficiently transfer the energy of light to the nearby semiconductor, causing enhanced absorption in the semiconductor at the location of the nanoparticles, or alternatively convert the light energy into a parasitic heat loss in the nanoparticle. Our model essentially captures the action of the electromagnetic field around the nanoparticles, which can lead to either the enhanced absorption in the semiconductor or a parasitic heat loss in the nanoparticle. We neglect the potential of the energetic charge carrier that is created in the nanoparticle being transferred to the semiconductor. This is a reasonable assumption since a large fraction of charge carriers formed in the nanoparticle lose their energy rapidly through the collisions with electrons or by exciting phonon modes (heating the nanoparticle).

To describe the optical behavior of a semiconductor, we use its complex refractive index ($n + i{\cdot}\kappa$). Figure S1 shows the wavelength-dependent values of κ and n for the TiO_2, $BiVO_4$, and Si semiconductors used in this work. We estimate the reflectance, R, using a simplified version of the Fresnel equation (eq S2) or experimentally published reflectance data (Figure S2) for a number of flat semiconductors. The Fresnel equation is most appropriate for flat and smooth surfaces (monocrystalline Si wafers) while experimental data are more appropriate for rough, particle-based surfaces (for example, films of TiO_2 and $BiVO_4$ nanoparticles). We use the Beer−Lambert Law, shown in eq 1, to compute the probability of photon absorption in the semiconductor as a function of the semiconductor depth.

$$A(\lambda, x) = 1 - \exp\left[-\frac{x}{d(\lambda)}\right] \tag{1}$$

The probability of absorption in the semiconductor, A, at a given wavelength, λ, is exponentially dependent on the quotient of the depth into the semiconductor, x, and the photon absorption depth, d. The photon absorption depth is defined as the distance at which the number of incident photons has been attenuated to 1/e of its initial number. This is equivalent to the reciprocal of the absorption coefficient and is dependent on the wavelength and the imaginary component of the refractive index (see the Supporting Information). In our PC model, none of the photons that traverse the entire semiconductor (i.e., are not absorbed) are reflected back into the semiconductor (i.e., they are transmitted) unless stated otherwise.

To account for the inclusion of plasmonic metal nanoparticles at a depth x_p in the semiconductor, we modify the semiconductor absorption probability calculation using eq 2. In this calculation, we assume that the photon energy that reaches the particle is either transferred into the SC at x_p (e.g., via LSPR-mediated near-field effect), producing energetic charge carriers in the SC at this depth, or it is dissipated as heat in the particle.[32,33]

$$A(\lambda, x) = \begin{cases} 1 - \exp\left[-\dfrac{x}{d(\lambda)}\right], & (0 \le x < x_p) \\ 1 - (1 - f_{et}(\lambda){\cdot}f_l)\exp\left[-\dfrac{x_p}{d(\lambda)}\right], & (x \ge x_p) \end{cases} \tag{2}$$

f_l is the probability of absorption in the semiconductor through the LSPR-mediated energy transfer process The sum of this probability (f_l) and the probability for the parasitic absorption in the metal (f_a) is assumed equal to 1. When f_l is 1, all the energy is injected into the SC. When f_l is 0, all the energy is dissipated as heat in the nanoparticle. An energy transfer parameter (f_{et}) is included to allow the plasmonic particle-induced transfer of energy to the semiconductor only when the incident photon energy is greater than the semiconductor band gap energy. It takes a value of 1 when the extinction coefficient (κ) of the semiconductor is $\ge 10^{-5}$ and a value of 0 when the extinction coefficient is $<10^{-5}$. This parameter essentially accounts for the fact that there will be no energy transfer if the semiconductor band gap energy is larger than the energy provided by the LSPR electric field; i.e., if the band gap in the semiconductor is too large, then there should be no energy transfer to the semiconductor. We use the value of 10^{-5} as a threshold since for this value of the extinction coefficient, even in the presence of large plasmonic field there would be relatively insignificant energy transfer to the semiconductor.

Photons are absorbed and generate charge carriers at various depths in the semiconductor in both the bare semiconductor

DOI: 10.1021/acs.jpcc.8b07214
J. Phys. Chem. C 2018, 122, 24279−24286

and composite semiconductor/metal cases. The probability of a charge carrier excited at a given semiconductor depth to recombine in the bulk of the semiconductor, before being collected by the catalyst at the electrode surface, is computed using eq 3

$$\mathrm{BR}(x) = 1 - \exp\left[-\frac{x}{L_\mathrm{d}}\right] \tag{3}$$

where x is the distance from the reactive surface in the semiconductor and L_d is the effective charge carrier diffusion length. The charge carrier diffusion length is a quantity used to account for the joint action of various recombination pathways including radiative, Auger, and Shockley−Read−Hall mechanisms.[34] This recombination probability depends on the type of band gap (e.g., direct or indirect), the doping concentration, and the magnitude of irradiance. For the particular materials analyzed in this work, we selected the typical charge carrier diffusion length from various published sources. In this simple approach to quantify the bulk recombination probability, the thickness of the depletion layer is assumed to be insignificant.

To simplify the model further and make it more physically tractable, we solve it in one dimension, i.e., for a slab of semiconductor where a plasmon "sheet" is introduced at a particular depth in the semiconductor. We use a 1-D grid to calculate the compounded probability of absorbing a photon at a given depth and successfully transporting the minority charge carrier to the reactive surface. This compounded probability for a given grid point (a slice of the semiconductor), C_i, is calculated using eq 4.

$$C_\mathrm{i}(\lambda, x[\sigma]) = [A(\lambda, x[\sigma]) - A(\lambda, x[\sigma - 1])]\cdot [1 - \mathrm{BR}(x[\sigma])] \tag{4}$$

Here, σ designates the specific grid point. C_i, which is incremental photon conversion probability, is the product of the incremental absorption probability at a given depth and the probability of the minority charge carrier successfully traveling back to the semiconductor surface from this depth. The cumulative photon conversion efficiency is calculated as the sum of each Ci over the entire semiconductor thickness and is equivalent to the EQE when multiplied by the probability of a photon not initially reflecting off the semiconductor surface (eq 5). The grid point at the front of the semiconductor surface is $\sigma = 1$, and the back of the semiconductor is at grid point $\sigma = \sigma_\mathrm{L}$. We note that we assume that a charge carrier that reaches the reactive site will cause a reaction, i.e., the EQE does not account for a reaction-specific energy requirements for charge carriers.

$$\mathrm{EQE}(\lambda) = [1 - R(\lambda)]\cdot \sum_{\sigma=1}^{\sigma=\sigma_\mathrm{L}} C_\mathrm{i}(\lambda, x[\sigma]) \tag{5}$$

Similarly, the absorptance by the semiconductor (i.e., ignoring the wasteful absorption by the metal nanoparticle), A_SC, is calculated with eq 6. It is the product of the fraction of photons that are not initially reflected and the probability of absorption over the entire semiconductor thickness, L.

$$A_\mathrm{SC}(\lambda) = [1 - R(\lambda)]\cdot A(\lambda, x = L) \tag{6}$$

Figure 1 provides a graphical demonstration of the PC model and the associated physical processes. The representative data in Figure 1a show the amount of absorption gained incrementally between each grid point. The processes shown in Figure 1b are drawn to directly correlate to the data in Figure 1a. In a bare semiconductor, the incremental absorption is greatest near the surface and decreases with increased depth. The remaining photons are transmitted through the semiconductor. In a semiconductor with a buried plasmonic sheet, the incremental absorption follows the same trajectory until the light reaches the nanoparticle at x_p. At this depth, the near-field effect (plasmonic energy transfer) completely redirects the photon energy to absorb in the semiconductor, or the energy is dissipated in the nanoparticle as heat. Beyond this depth, there is no additional absorption because we assume that the plasmonic sheet interacts with every photon. Once the photon energy is absorbed in the semiconductor, the resulting charge carrier will either diffuse to the catalytic site or recombine. The probability that the charge carrier reaches the catalytic site is quantified by 1 − the recombination probability and decreases as the depth into the semiconductor increases.

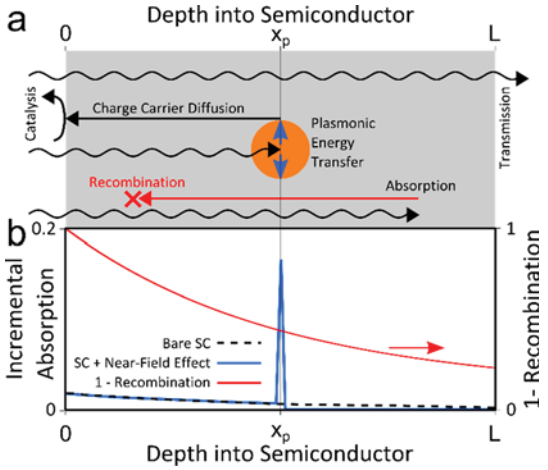

Figure 1. Graphical description of the PC model. (a) Illustration of the physical processes in the semiconductor. Light can be transmitted through the semiconductor or absorbed by the semiconductor due to the direct absorption or due to the energy transfer from a plasmonic nanoparticle. The energetic charge carriers can either reach the catalysts at the surface or recombine in the semiconductor. (b) The absorption gained incrementally between each grid point for a semiconductor with and without a buried plasmonic nanosheet is shown on the left axis. The probability of successful charge carrier transport (1 − recombination) is plotted relative to the right axis. The product of the incremental absorption and (1 − recombination) is equivalent to the incremental photon conversion probability (eq 4).

■ RESULTS AND DISCUSSION

Three classes of metal nanoparticles were investigated to study how the presence of the metal nanoparticles impacts the EQE: (1) parasitic, (2) ideal plasmonic, and (3) 50/50 plasmonic. In the parasitic case, f_l is set to zero, indicating that all photons reaching the metal nanoparticle are absorbed in the nanoparticle and dissipated as heat. In the ideal plasmonic case, f_l is set to 1, specifying that all photons interacting with the metal nanoparticle are absorbed in the semiconductor at that depth. This is essentially a perfect antenna that concentrates the energy and transfers it efficiently to the nearby semiconductor. The parasitic and ideal plasmonic classes represent lower and upper limits on the influence of metal nanoparticles on the EQE, respectively. In the 50/50 case, f_l is set to 0.5 to characterize a situation intermediate of the two limiting cases. This case is intended to represent a realistic plasmonic

DOI: 10.1021/acs.jpcc.8b07214
J. Phys. Chem. C 2018, 122, 24279−24286

nanoparticle that experiences LSPR at a given wavelength, dissipating half of the interacting photon energy as heat and injecting the other half into the semiconductor to excite charge carriers. We assume that these nanoparticles behave identically at all wavelengths; i.e., we assume that we can design plasmonic resonators across the UV−vis−NIR range.

In our analysis, we focus on three semiconductors (TiO_2, $BiVO_4$, and Si), which have different optical and charge transport properties. Figure S1 shows the optical characteristics of these semiconductors. In short, TiO_2 has a ∼3.2 eV direct band gap with a charge carrier diffusion length of ∼10 nm.[35,36] Monocrystalline Si has an indirect band gap of 1.12 eV, and it experiences direct electronic transitions for photon energies above ∼3.3 eV (i.e., an increase in the imaginary part of the refractive index). It has a charge carrier diffusion length between 100 and 400 μm.[26,34,37] $BiVO_4$ has a 2.4−2.5 eV indirect band gap, and it has direct electronic transitions that increase the imaginary part of the refractive index above ∼2.7 eV.[25,38,39] It has a charge carrier diffusion length of ∼100 nm.[38−40]

Case Study 1: Plasmonic Metal Nanoparticles Embedded in TiO_2. The data in Figure 2 show the effect of incorporating the three classes of metal nanoparticle sheets (parasitic, plasmonic, and 50/50) in a 500 μm thick TiO_2 photoelectrode. The charge carrier diffusion length of TiO_2 is set at 10 nm, and the plasmonic sheet is buried 10 nm into the TiO_2, matching the diffusion length. Introducing plasmonic nanoparticles farther from the surface and into the semiconductor would have no significant effect because a large fraction of the energetic charge carriers formed at these depths would recombine before reaching the surface.

The data in Figure 2a show that the parasitic and 50/50 metal nanoparticles hinder the absorptance in the semiconductor for short wavelengths (below ∼370 nm), and the ideal plasmonic case has no effect on the absorptance relative to bare TiO_2 at these wavelengths. The reason for this is that at these wavelengths, TiO_2 is a very good absorber (large imaginary part of the refractive index, κ) and the introduction of "lossy" metal nanoparticles can only have a negative effect. The absorptance of TiO_2 becomes weak above 370 nm as the band gap is approached (κ becomes smaller). At these wavelengths, the ideal plasmonic and 50/50 particles enhance the absorptance because light that would otherwise be absorbed far away from the surface is absorbed by the nanoparticles and a fraction of it is transferred to TiO_2. Here, a strong electric field around plasmonic materials would induce absorption in TiO_2 even when the extinction coefficient, κ, is very low. This enhancement disappears at wavelengths beyond the band gap due to the inability of the semiconductor to absorb light at these wavelengths ($\kappa \sim 0$), even with a strong near-field effect. The data in Figure 2b show how the resonant nanoparticles, positioned 10 nm below the TiO_2 surface, change the depth at which the photons are absorbed at the 360 nm wavelength. The data show that the ideal plasmonic and 50/50 cases shift the absorption of photons toward the regions that are closer to the surface of the semiconductor, where the probability of bulk recombination is much smaller. The parasitic case causes all photons remaining at the particle depth to be recombined.

Figure 2c shows the EQEs for the TiO_2 with the three different classes of metal nanoparticles embedded at a depth of 10 nm for wavelengths below the TiO_2 band gap (∼370 nm). The data show that the parasitic nanoparticle reduces the efficiency at all wavelengths, while the ideal plasmonic case enhances the EQE, regardless of the wavelength. At very short resonant wavelengths (less than ∼320 nm), the 50/50 nanoparticle hinders the efficiency. At these wavelengths, the

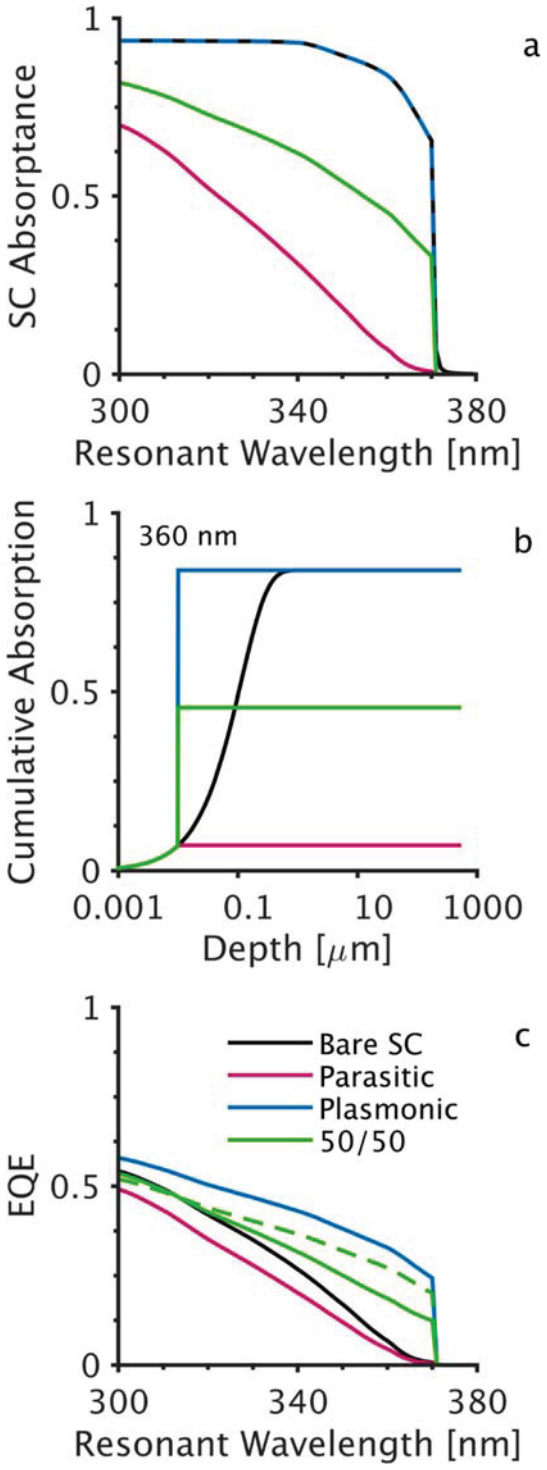

Figure 2. PC model calculations for 500 μm thick TiO_2 with plasmonic sheet buried 10 nm below the surface. (a) Absorptance in the TiO_2 part of the composite electrode. The bare and plasmonic results are identical for wavelengths below 370 nm. (b) Cumulative semiconductor absorption profile in the TiO_2 for a resonant wavelength of 360 nm. (c) Calculated EQEs for the different TiO_2 systems. The dashed green plot corresponds to the 50/50 particle buried 5 nm below the surface.

DOI: 10.1021/acs.jpcc.8b07214
J. Phys. Chem. C 2018, 122, 24279−24286

photon absorption depth in TiO_2 is very short (TiO_2 is an excellent absorber); therefore, the majority of photons are absorbed close to the surface, minimizing the role of bulk recombination. At longer wavelengths, where the absorption probability in TiO_2 starts to drop, the 50/50 particle improves the EQE, despite the fact that it reduces the total absorptance in the TiO_2 for most of these wavelengths (Figure 2a). Under these conditions, the 50/50 and ideal plasmonic particles induce the absorption process close to the surface, therefore limiting the role of bulk recombination. When the 50/50 particle is buried 5 nm below the surface, the EQE at short wavelengths decreases and the EQE at the long wavelengths increases, relative to the 10 nm deep 50/50 particle. These changes demonstrate that the particle should be buried close to the surface when the absorption depth is long relative to the diffusion length and short relative to the semiconductor thickness.

The data in Figure 2 show that plasmonic nanostructures can improve the performance of TiO_2 when positioned within one charge carrier diffusion length from the TiO_2 surface only at the wavelengths where the absorption rates in TiO_2 are relatively low. At the wavelengths where TiO_2 absorbs very well, it is difficult to envision that plasmonic nanostructures can be beneficial. We note that there have been experimental reports of plasmonic nanostructures improving the performance of TiO_2 or N-doped TiO_2 at wavelengths near the band gap.[21,23,28,41] The data shown in Figure 2 are in agreement with those experimental observations.

Case Study 2: Metal Nanoparticles Embedded in $BiVO_4$. $BiVO_4$ is characterized by a relatively large κ below ~480 nm which gradually decreases to 0 around 700 nm. The data in Figure 3 show the absorptance and EQE results for a 500 μm thick $BiVO_4$ photoelectrode. The metal nanoparticle depth and charge carrier diffusion length are both set to 100 nm.[38−40] In $BiVO_4$, the surface reflectance is the dominant source of optical loss at this thickness. Therefore, it is not surprising that the data in Figure 3a show that the plasmonic case accomplishes no absorptance enhancement at any wavelength and that the 50/50 and parasitic nanoparticles reduce the absorptance in $BiVO_4$ for every resonant wavelength. The reason for this is that at the thickness of 500 μm $BiVO_4$ will absorb all the light that is not reflected.

The data in Figure 3b show that the EQEs for the three metal nanoparticle cases at short wavelengths (below ~480 nm) show very little deviation from the EQE of the bare $BiVO_4$. The reason for this is that the photon absorption depth is short relative to the charge carrier diffusion length. At longer resonant wavelengths, the 50/50 case and, to a greater degree, the plasmonic case show moderate EQE enhancements. The reason for these EQE enhancements is that at these wavelengths the rate of absorption in $BiVO_4$ starts dropping (the photon absorption length increases), and the plasmonic nanostructures serve to ensure that the process of absorption takes place closer to the surface, therefore combating the recombination losses. These results suggest that realistic plasmonic metal nanoparticles, consisting of Ag or Au, that resonate above ~480 nm are expected to improve the EQE of $BiVO_4$ when these nanoparticles are buried within one diffusion length of the surface.

Case Study 3: Metal Nanoparticles Embedded in Si. The calculated absorptance and EQE for 500 μm thick Si photoelectrodes are shown in Figure 4a and Figure 4b, respectively. The metal nanoparticle depth and charge carrier diffusion length are both set to 100 μm. We note that charge carrier diffusion length of different types of crystalline Si electrodes can vary from 100 to 400 μm. At the 500 μm thickness, Si is a very efficient absorber across the visible spectrum and well into the infrared. Therefore, the introduction of a plasmonic structure can only improve the absorptance for photons above 1000 nm as shown in Figure 4a. These trends are preserved in the EQE results, with the plasmonic and 50/50 particles enhancing the EQE only at resonant wavelengths above 950 and 1000 nm, respectively. If the AM 1.5 solar spectrum (Figure S5) is the photon source, the enhancements achieved by the 50/50 particle in 500 μm thick Si are small due to the low intensities at these infrared wavelengths. Based on the data in Figure 4, we predict that that plasmonic metal nanostructure should have minimal utility when used with relatively thick Si samples. In these materials, it is much more beneficial to focus on reducing the surface reflection rates, which can be achieved by texturing the Si surface to direct the reflecting photons into the Si.[10,24,42−44]

While thick Si electrodes are very efficient absorbers that experience very little bulk recombination, thin Si electrodes are

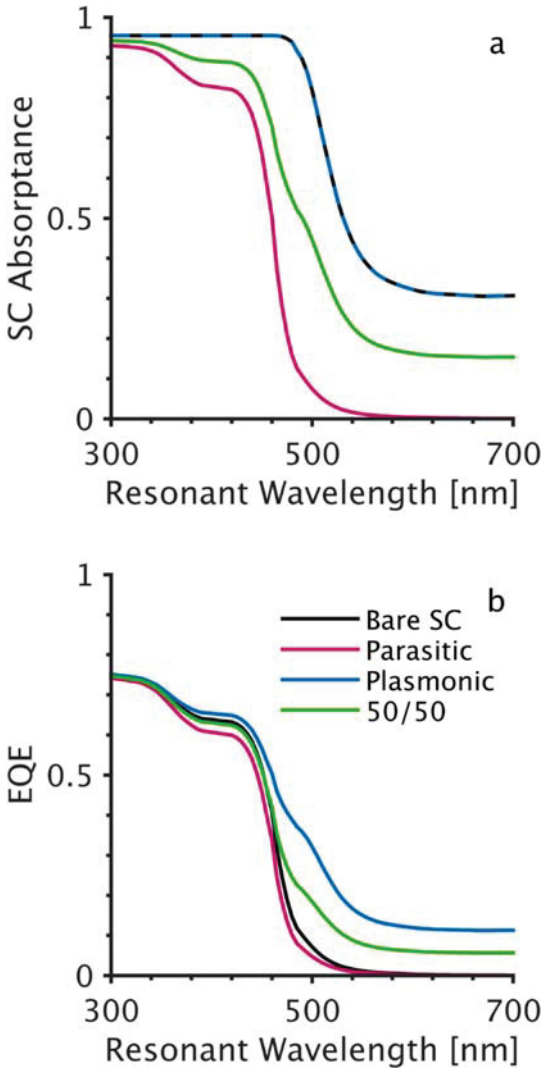

Figure 3. PC model calculations for 500 μm thick $BiVO_4$ with metal nanoparticles buried 100 nm below the surface. (a) Absorptance in the $BiVO_4$ part of the composite electrode. (b) Calculated EQEs for the different $BiVO_4$ systems.

DOI: 10.1021/acs.jpcc.8b07214
J. Phys. Chem. C 2018, 122, 24279−24286

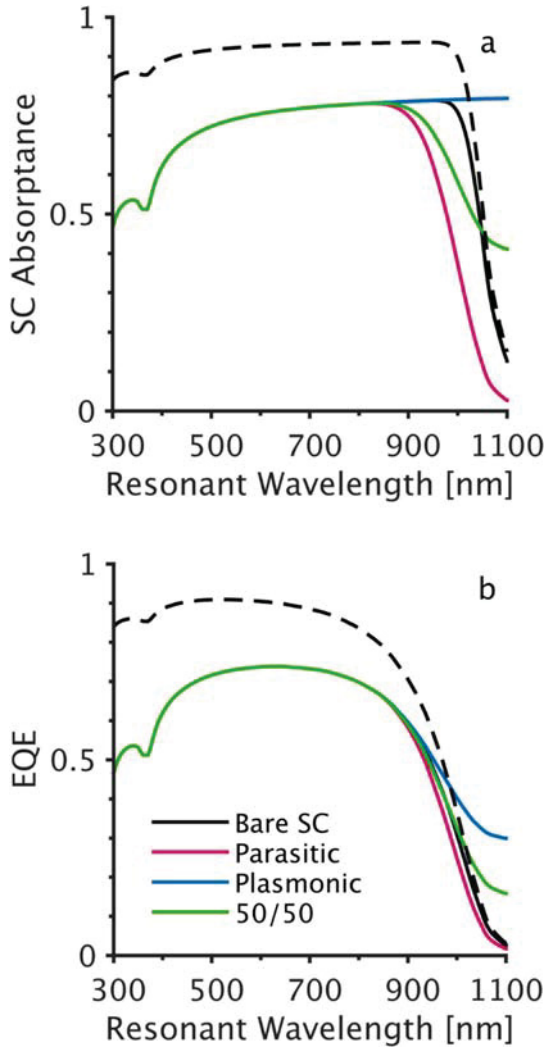

Figure 4. PC model calculations for 500 μm thick Si with metal nanoparticles buried 100 μm below the surface. (a) Absorptance in the Si part of the composite electrode. (b) Calculated EQEs for the different Si systems. The dashed plots correspond to a bare Si electrode with its reflectance reduced by 70%.

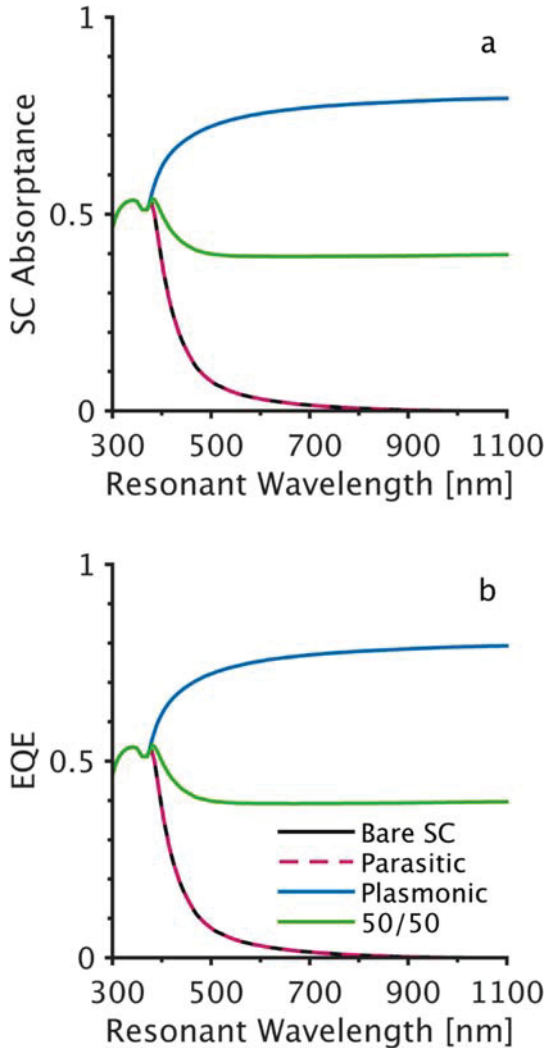

Figure 5. PC model calculations for 100 nm thick Si with metal nanoparticles buried 100 nm below the surface. (a) Absorptance in the Si part of the composite electrode. (b) Calculated EQEs for the different Si systems.

poor absorbers that maintain this low bulk recombination probability. Figure 5a and Figure 5b show the effect of placing metal nanoparticles at the back of a 100 nm thick Si photoelectrode on the Si absorptance and the EQE, respectively.

In this case, bulk recombination is negligible because the thickness of the electrode is 1000 times shorter than the diffusion length. As a result, the EQE changes are tied directly to how the metal nanoparticles change the absorptance in the Si. There are no optical efficiency losses that result from the inclusion of the parasitic and 50/50 particles because they are placed at the back of the electrode (i.e., they are only interacting with light that would otherwise be transmitted). At resonant wavelengths longer than 350 nm (where Si behaves as an indirect band gap semiconductor), the plasmonic and 50/50 cases strongly enhance the absorptance in the Si. The reason for this is that a large fraction of photons is absorbed at the back of the electrode rather than being transmitted.

Si is a fundamentally different type of semiconductor than TiO_2 and $BiVO_4$ in which bulk recombination losses are not the dominant loss mechanism, except at very long wavelengths. Instead, when the Si is thin, and therefore, a very poor absorber, realistic plasmonic metal nanoparticles are expected to improve the EQE through absorptance enhancements.

Generic Semiconductor. To further shed light on the impact of plasmonic nanostructures on various semiconductors, we have analyzed the behavior of a generic semiconductor in terms of reduced optical and geometric properties. The data in Figure 6 show the changes in EQE, induced by embedding a 50/50 plasmonic sheet, as a function of the reduced semiconductor thickness, particle depth, and charge carrier diffusion length. The reduced quantities are obtained by dividing these by the photon absorption depth. When the semiconductor is very thin relative to the photon absorption depth (Figure 6a, $L = 0.1$), the 50/50 particle improves the EQE for all realistic particle depths and diffusion lengths because the system is light absorption-limited. When the photon absorption depth and the semiconductor thickness are equal to each other (Figure 6b, $L = 1$), the 50/50 particle improves the EQE, except when the charge carrier diffusion length is very long (reduced diffusion length larger than 1) and the particle depth is short (i.e., plasmonic nanostructure at or close to the surface of the semiconductor). In the case of a very

DOI: 10.1021/acs.jpcc.8b07214
J. Phys. Chem. C 2018, 122, 24279−24286

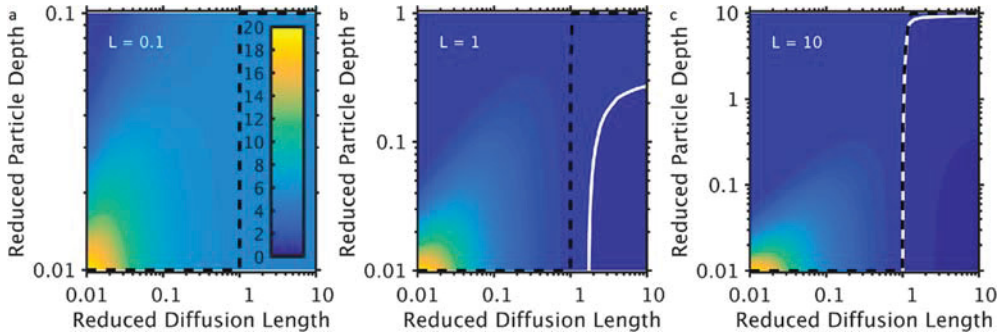

Figure 6. Generalized EQE enhancement factors (EQE with 50/50 particle divided by EQE of bare semiconductor) using reduced parameters relative to photon absorption depth. The black dashed line indicates the optimal 50/50 particle depth for a specific diffusion length. (a) Semiconductor thickness is 10 times shorter than the absorption depth. (b) Semiconductor thickness is equal to the absorption depth. (c) Semiconductor thickness is 10 times longer than the absorption depth. The color bar in Figure 6a applies to all three plots. The white contours show where the enhancement factor equals 1 (i.e., zero EQE change).

thick semiconductor (Figure 6c, $L = 10$) with a long diffusion length, there is negligible opportunity for EQE enhancement using a 50/50 particle; the system is already optimized. For these systems, the plasmonic nanoparticles can benefit the system only when the charge carrier diffusion length is relatively short (reduced diffusion length less than 1). For each of the semiconductor thicknesses shown, the particle depth should be minimized when the diffusion length is less than the absorption depth to maximize the EQE. When the diffusion length is greater than the absorption depth, the particle should be on the back side of the semiconductor to maximize the EQE by limiting parasitic losses.

■ CONCLUSIONS

We have developed a simple, physically tractable model to analyze the impact of plasmonic metal nanoparticles on the photon conversion efficiencies of semiconductors. The model captures the potentially positive impact of light harvesting by the nanostructures as well as the negative impact of the particle-induced parasitic dissipation of the incident electromagnetic energy into heat. The model provides us with a few guiding principles that should be followed when introducing plasmonic absorbers in a semiconductor. We find that the EQE of a semiconductor photoelectrode can be improved by buried plasmonic nanoparticles when there is at least one source of inefficiency derived from either poor absorption or high bulk recombination rates. The EQE of poorly absorbing semiconductors with low bulk recombination losses, such as thin Si, can be improved by placing plasmonic nanoparticles on the back of the electrode by reducing transmission losses. On the other hand when the charge carrier diffusion length is less than the photon absorption depth, the EQE can be improved by placing plasmonic nanostructures close to the surface of the semiconductor (i.e., where light is penetrating the semiconductor).

■ ASSOCIATED CONTENT

Supporting Information

The Supporting Information is available free of charge on the ACS Publications website at DOI: 10.1021/acs.jpcc.8b07214.

Optical properties of semiconductors and a detailed explanation of the PC model (PDF)

■ AUTHOR INFORMATION

Corresponding Author

*E-mail: linic@umich.edu.

ORCID

Paul A. Hernley: 0000-0002-2631-8880

Notes

The authors declare no competing financial interest.

■ ACKNOWLEDGMENTS

This work was primarily supported by the National Science Foundation (NSF) (CBET-1803991 and CBET-1702471). The synthesis was developed with the support of the U.S. Department of Energy, Office of Basic Energy Science, Division of Chemical Sciences (FG-02-05ER15686). Secondary support for the development of analytical tools used in the model was provided by NSF (CBET-1437601). S.L. also acknowledges the partial support of Technische Universität München–Institute for Advanced Study, funded by the German Excellence Initiative and the European Union Seventh Framework Programme under grant agreement n° 291763.

■ REFERENCES

(1) Sun, K.; Shen, S.; Liang, Y.; Burrows, P. E.; Mao, S. S.; Wang, D. Enabling Silicon for Solar-Fuel Production. *Chem. Rev.* **2014**, *114*, 8662–8719.

(2) Rossi, R. C.; Lewis, N. S. Investigation of the Size-Scaling Behavior of Spatially Nonuniform Barrier Height Contacts to Semiconductor Surfaces Using Ordered Nanometer-Scale Nickel Arrays on Silicon Electrodes. *J. Phys. Chem. B* **2001**, *105*, 12303–12318.

(3) Oh, J.; Deutsch, T. G.; Yuan, H.-C.; Branz, H. M. Nanoporous Black Silicon Photocathode for H_2 Production by Photoelectrochemical Water Splitting. *Energy Environ. Sci.* **2011**, *4*, 1690–1694.

(4) Aguiar, J. A.; Anderson, N. C.; Neale, N. R. Revealing the Semiconductor–Catalyst Interface in Buried Platinum Black Silicon Photocathodes. *J. Mater. Chem. A* **2016**, *4*, 8123–8129.

(5) Gorostiza, P.; Servat, J.; Morante, J. R.; Sanz, F. First Stages of Platinum Electroless Deposition on Silicon (100) from Hydrogen Fluoride Solutions Studied by AFM. *Thin Solid Films* **1996**, *275*, 12–17.

(6) Huang, Z.; McKone, J. R.; Xiang, C.; Grimm, R. L.; Warren, E. L.; Spurgeon, J. M.; Lewerenz, H.-J.; Brunschwig, B. S.; Lewis, N. S. Comparison between the Measured and Modeled Hydrogen-Evolution Activity of Ni- or Pt-Coated Silicon Photocathodes. *Int. J. Hydrogen Energy* **2014**, *39*, 16220–16226.

DOI: 10.1021/acs.jpcc.8b07214
J. Phys. Chem. C 2018, 122, 24279–24286

(7) Esposito, D. V.; Levin, I.; Moffat, T. P.; Talin, A. A. H_2 Evolution at Si-Based Metal-Insulator-Semiconductor Photoelectrodes Enhanced by Inversion Channel Charge Collection and H Spillover. *Nat. Mater.* **2013**, *12*, 562−568.
(8) Kye, J.; Shin, M.; Lim, B.; Jang, J.-W.; Oh, I.; Hwang, S. Platinum Monolayer Electrocatalyst on Gold Nanostructures on Silicon for Photoelectrochemical Hydrogen Evolution. *ACS Nano* **2013**, *7*, 6017−6023.
(9) Lombardi, I.; Marchionna, S.; Zangari, G.; Pizzini, S. Effect of Pt Particle Size and Distribution on Photoelectrochemical Hydrogen Evolution by P-Si Photocathodes. *Langmuir* **2007**, *23*, 12413−12420.
(10) Hernley, P. A.; Chavez, S. A.; Quinn, J. P.; Linic, S. Engineering the Optical and Catalytic Properties of Co-Catalyst/Semiconductor Photocatalysts. *ACS Photonics* **2017**, *4*, 979−985.
(11) Bae, D.; Pedersen, T.; Seger, B.; Malizia, M.; Kuznetsov, A.; Hansen, O.; Chorkendorff, I.; Vesborg, P. C. K. Back-Illuminated Si Photocathode: A Combined Experimental and Theoretical Study for Photocatalytic Hydrogen Evolution. *Energy Environ. Sci.* **2015**, *8*, 650−660.
(12) Kay, A.; Cesar, I.; Grätzel, M. New Benchmark for Water Photooxidation by Nanostructured Alpha-Fe_2O_3 Films. *J. Am. Chem. Soc.* **2006**, *128*, 15714−15721.
(13) Wiley, B. J.; Im, S. H.; Li, Z.-Y.; McLellan, J.; Siekkinen, A.; Xia, Y. Maneuvering the Surface Plasmon Resonance of Silver Nanostructures through Shape-Controlled Synthesis. *J. Phys. Chem. B* **2006**, *110*, 15666−15675.
(14) Linic, S.; Christopher, P.; Ingram, D. B. Plasmonic-Metal Nanostructures for Efficient Conversion of Solar to Chemical Energy. *Nat. Mater.* **2011**, *10*, 911−921.
(15) Zhang, X.; Chen, Y. L.; Liu, R.-S.; Tsai, D. P. Plasmonic Photocatalysis. *Rep. Prog. Phys.* **2013**, *76*, No. 046401.
(16) Evanoff, D. D.; Chumanov, G. Synthesis and Optical Properties of Silver Nanoparticles and Arrays. *ChemPhysChem* **2005**, *6*, 1221−1231.
(17) Mahmoud, M. A. E. M.; Chamanzar, M.; Adibi, A.; El-Sayed, M. A. Effect of the Dielectric Constant of the Surrounding Medium and the Substrate on the Surface Plasmon Resonance Spectrum and Sensitivity Factors of Highly Symmetric Systems; Silver Nanocubes. *J. Am. Chem. Soc.* **2012**, *134*, 6434−6442.
(18) Aslam, U.; Chavez, S.; Linic, S. Controlling Energy Flow in Multimetallic Nanostructures for Plasmonic Catalysis. *Nat. Nanotechnol.* **2017**, *12*, 1000−1005.
(19) Christopher, P.; Xin, H.; Linic, S. Visible-Light-Enhanced Catalytic Oxidation Reactions on Plasmonic Silver Nanostructures. *Nat. Chem.* **2011**, *3*, 467−472.
(20) Savage, K. J.; Hawkeye, M. M.; Esteban, R.; Borisov, A. G.; Aizpurua, J.; Baumberg, J. J. Revealing the Quantum Regime in Tunnelling Plasmonics. *Nature* **2012**, *491*, 574−577.
(21) Ingram, D. B.; Linic, S. Water Splitting on Composite Plasmonic-Metal/Semiconductor Photoelectrodes: Evidence for Selective Plasmon-Induced Formation of Charge Carriers near the Semiconductor Surface. *J. Am. Chem. Soc.* **2011**, *133*, 5202−5205.
(22) Thomann, I.; Pinaud, B. A.; Chen, Z.; Clemens, B. M.; Jaramillo, T. F.; Brongersma, M. L. Plasmon Enhanced Solar-to-Fuel Energy Conversion. *Nano Lett.* **2011**, *11*, 3440−3446.
(23) Lai, Y.; Zhuang, H.; Xie, K.; Gong, D.; et al. Fabrication of Uniform Ag/TiO_2 Nanotube Array Structures with Enhanced Photoelectrochemical Performance. *New J. Chem.* **2010**, *34*, 1335−1340.
(24) Pillai, S.; Catchpole, K.; Trupke, T.; Green, M. A. Surface Plasmon Enhanced Silicon Solar Cells. *J. Appl. Phys.* **2007**, *101*, No. 093105.
(25) Abdi, F. F.; Dabirian, A.; Dam, B.; van de Krol, R. Plasmonic Enhancement of the Optical Absorption and Catalytic Efficiency of $BiVO_4$ Photoanodes Decorated with Ag@SiO_2 Core−shell Nanoparticles. *Phys. Chem. Chem. Phys.* **2014**, *16*, 15272−15277.
(26) Atwater, H. A.; Polman, A. Plasmonics for Improved Photovoltaic Devices. *Nat. Mater.* **2010**, *9*, 205−213.
(27) Cushing, S. K.; Bristow, A. D.; Wu, N. Theoretical Maximum Efficiency of Solar Energy Conversion in Plasmonic Metal-Semiconductor Heterojunctions. *Phys. Chem. Chem. Phys.* **2015**, *17*, 30013−30022.
(28) Wang, H.; You, T.; Shi, W.; Li, J.; Guo, L. Au/TiO_2/Au as a Plasmonic Coupling Photocatalyst. *J. Phys. Chem. C* **2012**, *116*, 6490−6494.
(29) Schaadt, D. M.; Feng, B.; Yu, E. T. Enhanced Semiconductor Optical Absorption via Surface Plasmon Excitation in Metal Nanoparticles. *Appl. Phys. Lett.* **2005**, *86*, No. 063106.
(30) Gao, H.; Liu, C.; Jeong, H. E.; Yang, P. Plasmon-Enhanced Photocatalytic Activity of Iron Oxide on Gold Nanopillars. *ACS Nano* **2012**, *6*, 234−240.
(31) Chen, C.-J.; Chen, M.-G.; Chen, C. K.; Wu, P. C.; Chen, P.-T.; Basu, M.; Hu, S.-F.; Tsai, D. P.; Liu, R.-S. Ag-Si Artificial Microflowers for Plasmon-Enhanced Solar Water Splitting. *Chem. Commun. (Cambridge, U. K.)* **2015**, *51*, 549−552.
(32) Khurgin, J. B. How to Deal with the Loss in Plasmonics and Metamaterials. *Nat. Nanotechnol.* **2015**, *10*, 2−6.
(33) Theuring, M.; Wang, P. H.; Vehse, M.; Steenhoff, V.; von Maydell, K.; Agert, C.; Brolo, A. G. Comparison of Ag and SiO_2 Nanoparticles for Light Trapping Applications in Silicon Thin Film Solar Cells. *J. Phys. Chem. Lett.* **2014**, *5*, 3302−3306.
(34) Tyagi, M. S.; Van Overstraeten, R. Minority Carrier Recombination in Heavily-Doped Silicon. *Solid-State Electron.* **1983**, *26*, 577−597.
(35) Hodes, G.; Kamat, P. V. Understanding the Implication of Carrier Diffusion Length in Photovoltaic Cells. *J. Phys. Chem. Lett.* **2015**, *6*, 4090−4092.
(36) Grätzel, M. Photoelectrochemical Cells. *Nature* **2001**, *414*, 338−344.
(37) Boettcher, S. W.; Spurgeon, J. M.; Putnam, M. C.; Warren, E. L.; Turner-Evans, D. B.; Kelzenberg, M. D.; Maiolo, J. R.; Atwater, H. A.; Lewis, N. S. Energy-Conversion Properties of Vapor-Liquid-Solid-Grown Silicon Wire-Array Photocathodes. *Science* **2010**, *327*, 185−187.
(38) Cooper, J. K.; Gul, S.; Toma, F. M.; Chen, L.; Liu, Y. S.; Guo, J.; Ager, J. W.; Yano, J.; Sharp, I. D. Indirect Bandgap and Optical Properties of Monoclinic Bismuth Vanadate. *J. Phys. Chem. C* **2015**, *119*, 2969−2974.
(39) Kim, T. W.; Choi, K.-S. K.-S. Nanoporous $BiVO_4$ Photoanodes with Dual-Layer Oxygen Evolution Catalysts for Solar Water Splitting. *Science* **2014**, *343*, 990−994.
(40) Rettie, A. J. E.; Lee, H. C.; Marshall, L. G.; Lin, J.-F.; Capan, C.; Lindemuth, J.; McCloy, J. S.; Zhou, J.; Bard, A. J.; Mullins, C. B. Combined Charge Carrier Transport and Photoelectrochemical Characterization of $BiVO_4$ Single Crystals: Intrinsic Behavior of a Complex Metal Oxide. *J. Am. Chem. Soc.* **2013**, *135*, 11389−11396.
(41) Christopher, P.; Ingram, D. B.; Linic, S. Enhancing Photochemical Activity of Semiconductor Nanoparticles with Optically Active Ag Nanostructures: Photochemistry Mediated by Ag Surface Plasmons. *J. Phys. Chem. C* **2010**, *114*, 9173−9177.
(42) Branz, H. M.; Yost, V. E.; Ward, S.; Jones, K. M.; To, B.; Stradins, P. Nanostructured Black Silicon and the Optical Reflectance of Graded-Density Surfaces. *Appl. Phys. Lett.* **2009**, *94*, 231121.
(43) Zhao, Y.; Anderson, N. C.; Zhu, K.; Aguiar, J. A.; Seabold, J. A.; Van De Lagemaat, J.; Branz, H. M.; Neale, N. R.; Oh, J. Oxidatively Stable Nanoporous Silicon Photocathodes with Enhanced Onset Voltage for Photoelectrochemical Proton Reduction. *Nano Lett.* **2015**, *15*, 2517−2525.
(44) Kelzenberg, M. D.; Boettcher, S. W.; Petykiewicz, J. A.; Turner-Evans, D. B.; Putnam, M. C.; Warren, E. L.; Spurgeon, J. M.; Briggs, R. M.; Lewis, N. S.; Atwater, H. A. Enhanced Absorption and Carrier Collection in Si Wire Arrays for Photovoltaic Applications. *Nat. Mater.* **2010**, *9*, 239−244.

DOI: 10.1021/acs.jpcc.8b07214
J. Phys. Chem. C 2018, 122, 24279−24286